A COMPREHENSIVE INVESTIGATION OF THE STRUCTURAL AND MAGNETIC BEHAVIOR OF CTAB-COATED NiCuZn SPINEL NANO FERRITE

Abstract

The spinel nano ferrite with elemental composition $Ni_{0.3}Cu_{0.3}Zn_{0.4}Fe_2O_4$ and CTAB-coated $Ni_{0.3}Cu_{0.3}Zn_{0.4}Fe_2O_4$was prepared using the co-precipitation method. The modification in microstructural, magnetic, and dielectric properties was recorded by X-ray diffraction (XRD), Vibrating Sample Magnetometer (VSM), and Impedance Spectroscopy. The X-ray diffraction pattern with a prominent (311) plane confirms spinel ferrite with space group Fd-3m. Additionally, the intensity ranges from 569-1797cps and the 2θ position is between 35.571°-35.626°, indicating a more ordered structure of spinel ferrite with CTAB. The modification in the structural parameter was observed through crystallite size(18-25nm), strain ($6.240x10^{-3}$-$4.383x10^{-3}$), dislocation density ($3.023x10^{15}$-$1.496x10^{15}1/m^2$), packing factor (72.113-102.746), lattice dimension (8.3638-8.3433A°), stacking fault (0.448-0.446), X-ray density (5.417-5.457 g/cm^3), experimental density (2.861-3.253 g/cm^3), specific surface area ($60.90\ x10^3$ -$42.53\ x10^3$ m^2/g) and % porosity (47.18-40.38). Additionally, this research explores the relationship between magnetic properties and X-ray diffraction analysis. Interionic distances (p, q, r, s, b, c, d, e, f) and bond angles (θ_1, θ_2, θ_3, θ_4, and θ_5) were calculated to determine A-A, A-B, and B-B interactions for all samples. The recorded strong vibrations within the range of 400-600 cm^{-1} using FTIR confirm the presence of the Fe-O functional group of spinel ferrite in all the materials that were prepared. The smooth magnetic isotherm (M-H loop) with coercivity (165.661-75.231Oe), magnetic saturation (41.469-61.880 emu/g), retentivity (9.730-5.526 emu/g), magnetic anisotropy

Authors

Shrikant M. Suryawanshi
Department of Physics
Kamla Nehru Mahavidyalaya
Nagpur, India.

Dilip S. Badwaik
Department of Physics
Kamla Nehru Mahavidyalaya
Nagpur, India.
badwaik_ds@rediffmail.com

Sarang R. DAF
Department of Physics
Kamla Nehru Mahavidyalaya
Nagpur, India.

Pooja A. Zingare
Department of Physics
Kamla Nehru Mahavidyalaya
Nagpur, India.

Pushpalata S. Hedaoo
Department of Physics
RTMNU
Nagpur, India.

Lalit D. Channe
Department of Physics
Hislop College
Nagpur, India.

(7010-4398 erg/cm^3) and magnetic moment (1.770-2.6420μ_B) corresponds to elevation in spin-orbit interaction, noncollinear arrangement of surface spins and spin canting in the sublattice respectively. The squareness ratio in the range of 0.217-0.096 indicates that the prepared nano ferrite is of a pseudo-single domain nature and suitable for Multilayer Chip Inductor (MLCI) application.

Keywords: $Ni_{0.3}Cu_{0.3}Zn_{0.4}Fe_2O_4$, CTAB, XRD, VSM

I. INTRODUCTION

Magnetic materials in nanoscale have become increasingly popular in recent years due to their superior performance in catalytic, thermal, mechanical, optical, and electrical applications compared to bulk magnetic materials. Magnetic nanoparticles or nanomagnetic materials have distinct chemical compositions, and various types have been developed and used for different applications [1].

The magnetic properties of nanoparticles are mainly influenced by two characteristics: (a) Finite-size effects, which can either be single-domain or multi-domain structures, and the quantum confinement of electrons; (b) Surface effects, which result from the breaking of symmetry at the surface of a particle's crystal structure, the presence of surfactants, dangling bonds, surface strain, oxidation, or even different chemical and physical structures of the internal-core and surface-shell parts of the nanoparticle. As the size of the nanoparticles decreases, the ratio of surface-to-volume increases. As a result, the magnetic moment per atom and the magnetic anisotropy of nanoparticles may differ from that of a bulk specimen [2]. The Curie (Tc) or Neel (T_N) temperatures, and the coercivity (Hc) are among the magnetic properties that differ from the bulk material. In the bulk ferromagnetic material, small regions of magnetic domains are present due to a balance of various energy terms, such as the exchange energy, magnetocrystalline anisotropy, and magnetostatic (or dipolar) energy [3,4]. Studies have shown that ferromagnetic crystals possess magnetic domains that have a critical size of approximately 100 nm. These domains, known as single-domain particles, cannot split up further into smaller domains [5, 6, 7].

Magnetic nanoparticles (MNPs) are a type of nanoparticles (NPs) that react to a magnetic field when it is applied. When the size of magnetic nanoparticles (MNPs) drops below a certain limit, they may consist of a single magnetic domain. At a particular temperature, known as the blocking temperature (TB), MNPs display superparamagnetic behavior which means they respond quickly to changes in the magnetic field without any remnant magnetization or coercivity. MNPs in the superparamagnetic state behave like paramagnetic atoms with a giant spin[8,9]. Magnetic nanoparticles (MNPs) possess a number of distinctive magnetic properties, including superparamagnetism, high magnetic susceptibility, and low Curie temperature. As a result, these materials are utilized in a variety of industrial, medical, and environmental applications, such as medical diagnosis and treatment, magnetic fluids, biomedicine, catalysis, magnetic energy storage, data storage, and magnetic resonance imaging (MRI), etc.

Spinel Ferrite and its Applications: Spinel ferrite, also known as cubic ferrite, is a magnetic material with a cubic crystal structure that is widely used in the ferrite family. Its high electrical resistivity and low eddy current losses make it an ideal choice for use in microwave frequencies. [10]. Spinel ferrites have the general formula MFe_2O_4 (where M is divalent metal cations such as Fe^{2+}, Mn^{2+}, Co^{2+}, Ni^{2+}, Zn^{2+}, $Cu^{2+,}$ etc., or a combination of these ions and belongs to space group Fd-3m, that is derived from the crystal structure of natural mineral spinel $MgAl_2O_4$ was first determined by Bragg and Nishikawa in 1915. In spinel ferrites, 32 oxygen atoms form a unit cell having a face-centered cubic (FCC) structure arrangement leaving tetrahedral sites (A) and octahedral sites [B], that are surrounded by four and six oxygen atoms respectively. The FCC structure of spinel ferrites contains 64 tetrahedral sites (A) and 32 octahedral sites [B]. To maintain the electrical neutrality of the

lattice, there are one-eighth of the tetrahedral sites (A) and one-half of the octahedral sites [B] are occupied by the cations in a unit cell [11].

Spinel ferrite magnetic nanoparticles with tuneable electric and magnetic properties show various industrial applications reported by researchers. C. Yang et al.[12] discussed the use of spinel ferrite as inductive components in a wide range of electronic circuits, including low-noise amplifiers, filters, voltage-controlled oscillators, and impedance-matching networks. According to S. Bae et al.[13], MFe_2O_4 (M-Co, Mg, Mn) is a crucial element used in cellular phones, video cameras, notebook computers, floppy drives, and thermistors. Power application of Ni-Zn and Mn-Zn ferrite reported by A. Verma et.al [14]. The high-frequency application of Ni-Mn spinel ferrite was reported by N. Channa et.al [15]. P. Smitha et al.[16] reported on the efficacy of spinel ferrite as a radar-absorbing material. B.Bhujun et. al[17] reported Aluminium doped spinel ferrite electrodes for supercapacitors, etc. In addition to such electronic or industrial applications, spinel ferrite has received a considerable amount of attention in the biomedical field also[18-20]. The contributions of spinel ferrite in various medical diagnosis is also reported by researchers. A. Benali et. al[21] reported $CoFe_2O_4$ spinel ferrite studies on permanent magnet application and cytotoxic effects on breast and prostate cancer cell lines. S. B. Somvanshi et.al [22] develop spinel ferrite magnetic nanoparticle for COVID-19 detection and multifunctional nanoporous magnetic zinc silicate-$ZnFe_2O_4$ core-shell composite for bone tissue engineering applications reported by A. Bigham et.al [23] etc.

Thus, the overall multifunctional properties of spinel ferrite that have been reported may have specific Physio-chemical parameters that can be achieved by choice of stoichiometric ratio, Synthesis method, calcination, pH, and capping agent. The spinel ferrite can be synthesized by sol-gel auto combustion, hydrothermal method, co-precipitation method, and many more physical and chemical methods. Out of all, co-precipitation is a simple technique to synthesize the ferrite nanoparticles at low temperatures with high purity appropriate for magnetic characterization [24]. Although the co-precipitation approach is the convenient and traditional method for the production of spinel nano ferrite, it is difficult to control microstructural parameters. It can be achieved with the proper modification in the synthesis approach by the introduction of capping agents having surface tension-reducing properties [25]. In the present research module, CTAB-coated NiCuZn spinel nano ferrite synthesized by coprecipitation was taken under investigation. The modification in microstructural, magnetic, and dielectric properties was recorded using X-ray diffraction analysis (XRD), Vibrating sample Magnetometer (VSM), and Impedance spectroscopy.

II. SYNTHESIS OF MATERIAL AND CHARACTERIZATION TOOLS

The $Ni_{0.3}Cu_{0.3}Zn_{0.4}Fe_2O_4$ and CTAB-coated $Ni_{0.3}Cu_{0.3}Zn_{0.4}Fe_2O_4$ spinel nano ferrites were prepared using the coprecipitation method. A combined divalent metal ions solution (0.2 M of Nickel Chloride (II) $NiCl_2.6H_2O$, Copper Chloride (II) $CuCl_2.2H_2O$, and Zinc Chloride (II) $ZnCl_2$), and trivalent metal ion solution (0.4M of Iron chloride (III) $FeCl_3$) were taken separately in 40 ml of double distilled water followed by stirring about 15 min to get a homogeneous solution. For the preparation of $Ni_{0.3}Cu_{0.3}Zn_{0.4}Fe_2O_4$, divalent(NiCuZn) and trivalent(Fe) solutions mixed together, heat at 80°C and stir with the addition of NaOH (4M) to get pH-12.The same procedure was followed with the addition of 0.2M and 0.4 M CTAB in mixed metal ions solution and maintained pH-12.The resultant solution of

$Ni_{0.3}Cu_{0.3}Zn_{0.4}Fe_2O_4$, CTAB(0.2M)-$Ni_{0.3}Cu_{0.3}Zn_{0.4}Fe_2O_4$ and CTAB(0.4M)-$Ni_{0.3}Cu_{0.3}Zn_{0.4}Fe_2O_4$ was filtered by double distilled water and ethanol 3-5 times and dried for 2hr at 100°C in an oven. The dried material was grind for 3 hrs using mortar-pestle. The obtained material was calcinated at 800°C for 5hr, and grind for 1hr to get powder form. The final samples were coded as SF, SF- CTAB @ 0.2, and SF-CTAB@ 0.4 in accordance with the molar concentration of CTAB in synthesized spinel ferrite respectively.

The microstructural properties of SF, SF-CTAB@0.2, and SF-CTAB@ 0.4 were recorded using an X-Ray diffractometer (Bruker D8 Advance) (λ=1.5406 Å). The functional group analysis was observed by Fourier Transform Infrared Spectroscopy (FTIR) within 450 $cm^{-1}$to 4000cm^{-1} using Model - Agilent Cary 630 FTIR Spectrometer. The magnetic properties were investigated using a M-H loop using Vibrating Sample Magnetometer (VSM) (Lakeshore 7400 series) and dielectric properties were recorded by Impedance spectroscopy (Model: Waynekerr, 6500 B)

III. RESULTS AND DISCUSSION

1. X-ray Diffraction Analysis

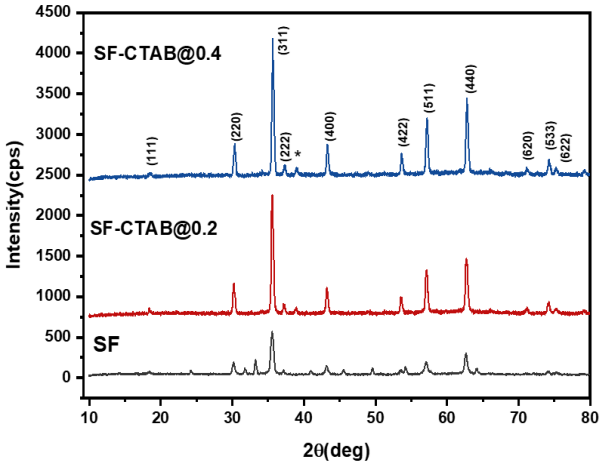

Figure 1A: Comparative X-ray diffraction pattern of prepared SF, SF-CTAB@0.2, and SF-CTAB@0.4

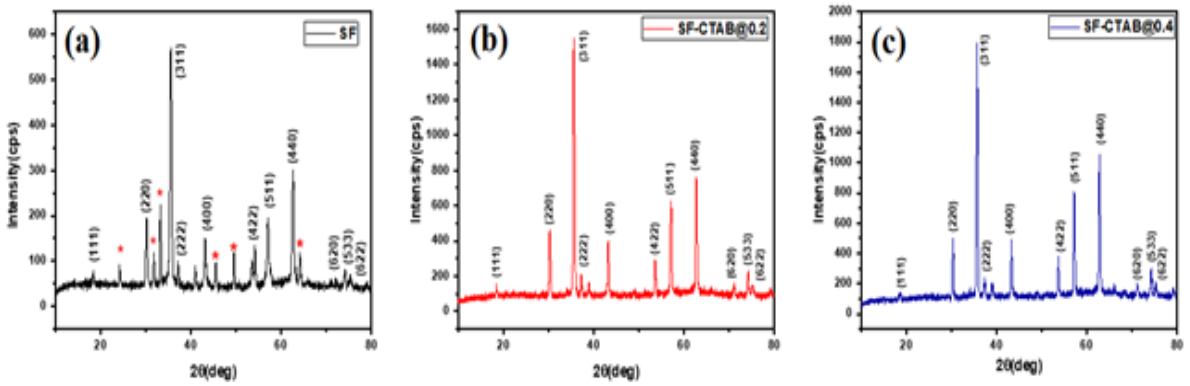

Figure 1B: X-ray diffraction pattern of prepared (a)SF, (b)SF-CTAB@0.2, and (c)SF-CTAB@0.4

The microstructural properties of prepared $Ni_{0.3}Cu_{0.3}Zn_{0.4}Fe_2O_4$ (SF, SF-CTAB@0.2, and SF-CTAB@ 0.4) were demonstrated by X-ray diffraction analysis (**Figure.1A**.). The recorded diffraction at (111), (220), (311), (222), (400), (422), (511) and (440) corresponds to cubic/spinel ferrite material (space group Fd-3m). The observed higher (311) peak with intensity 569, 1549, and 1797 cps for SF, SF-CTAB@0.2, and SF-CTAB@ 0.4 corresponds to the more ordered structure of SF-CTAB@ 0.4 than SF, SF-CTAB@0.2 accordingly(**Figure.1B**). The X-ray intensity was also used to determine the site preference of divalent and trivalent metal ions or cation distribution in spinel ferrite according to P.P. Hankare et.al [26]. The indexed (220), (400), (422), and (440) were considered to be structure-sensitive planes in the spinel ferrite system. The change in cation at tetrahedral(A) sites is sensitive to (220) and (400), while (222) is sensitive to the octahedral site and the (511) plane is sensitive to the oxygen ion u parameter [27]. The remaining (422), and (440) are sensitive to cations at tetrahedral(A) and octahedral [B] sites, however, cation distribution is not affected by the most intense (311) plane because of its independence towards oxygen positional parameter and cation distribution, reported by B. B. V. S. Vara Prasad et.al [28]. The effect of capping agent (CTAB) on the cation distribution of prepared materials was calculated through intensity ratio of $I_{(400)}/I_{(220)}$, $I_{(400)}/I_{(422)}$, $I_{(440)}/I_{(422)}$ and $I_{(440)}/I_{(220)}$ and estimated in **Table 1.**

Table 1: Intensity of (311),(222) and (511) plane and ratio of intensity corresponds to (400),(440) and (220) of prepared SF, SF-CTAB@0.2 and SF-CTAB@0.4

Samples	**$I_{(311)}$**	**$I_{(222)}$**	**$I_{(511)}$**	**$I_{(400)}/I_{(220)}$**	**$I_{(400)}/I_{(422)}$**	**$I_{(440)}/I_{(422)}$**	**$I_{(440)}/I_{(220)}$**
SF	569	99	196	0.771	1.455	2.885	1.528
SF-CTAB@0.2	1549	210	627	0.876	1.391	2.628	1.655
SF-CTAB@0.4	1797	238	814	0.976	1.276	2.757	2.080

Table.1 shows significant variation in $I_{(400)}/I_{(220)}$, $I_{(400)}/I_{(422)}$, $I_{(440)}/I_{(422)}$, and $I_{(440)}/I_{(220)}$, indicating migration of divalent (Ni, Cu, Zn) and trivalent (Fe) between tetrahedral and octahedral sites. The modification in $I_{(400)}/I_{(220)}$, $I_{(400)}/I_{(422)}$, $I_{(440)}/I_{(422)}$, and $I_{(440)}/I_{(220)}$ from SF to SF-CTAB@0.4 corresponds to improved crystallinity, crystallite size, strain, and defects.

The microstructural parameters, including crystallite size (D), strain (ε), dislocation density (δ), lattice dimension (a), packing factor (PF), stacking fault ($F_{Staking}$), X-ray density (ρ_{X-ray}), and specific surface area (S_{Area}), were calculated for the most intense (311) plane using **Eq.(1)** to **Eq.(8)** and are summarized in **Table.2** and **3**.

$$D = \frac{0.9\lambda}{\beta \cos\theta} \quad (1)$$

$$a = d_{hkl}\sqrt{h^2 + k^2 + l^2} \quad (2)$$

$$\delta = {}^{1}\!\!\diagup\!\!{}_{D^2} \quad (3)$$

$$\varepsilon = \frac{\beta}{4\tan\theta} \quad (4)$$

$$PF = \frac{D}{d-spacing} \quad (5)$$

$$F_{stacking} = \frac{2\pi^2}{45\sqrt{3\tan\theta}} \quad (6)$$

$$S_{Area} = \frac{6}{D \times \rho_{X-ray}} \quad (7)$$

$$\rho_{X-ray} = \frac{ZM}{N_A a^3} \quad (8)$$

Where *D* is crystallite size, β is FWHM, λ = 1.54060 Å and θ is related to the peak position, Z (For spinel ferrite Z = 8) is the number of molecules per unit cell. M specifies the molecular weight of synthesized material, N_A = 6.02 × 10^{23} 1/mol is Avogadro's number.

Table 2: Peak position (2θ), FWHM (β), Interplanar spacing (d-spacing), Crystallite Size (D), Lattice dimension (a) and cell volume (V) of prepared SF, SF-CTAB@0.2 and SF-CTAB@0.4 nano ferrite

Samples	***2θ*(deg)**	***B*(deg)**	***d*-spacing (Å)**	***D* (nm)**	***a* (Å)**	***V* (Å^3)**
SF	35.571	0.459	2.5218	18.185	8.3638	585.074
SF-CTAB@0.2	35.564	0.354	2.5223	23.579	8.3655	585.430
SF-CTAB@0.4	35.626	0.323	2.5156	25.846	8.3433	580.782

As estimated in **Table.2,** The crystallite size(D) of prepared material found to be increased (18 nm-25nm) from SF to SF-CTAB@0.4 corresponds to improved crystallization due reduction of surfactant/capping agent (CTAB)activity. The effect of CTAB on crystallite size is determined by concentration-dependent surfactant-particles and surfactant-surfactant interactions. Lower concentrations reduce surface tension and envelope nucleating particles, resulting in smaller crystallites. Higher concentrations lead to reduced surfactant activity and larger crystallites, according to M. Haneef et al. [29]. The lattice dimension for SF-CTAB@0.2 (8.3655 Å) was higher than SF (8.3638 Å) and SF-CTAB@0.4 (8.3433 Å). This can be linked to lattice strain caused by dislocations in SF, SF-CTAB@0.2, and SF-CTAB@0.4 respectively.

The decrease in dislocation density(total number of dislocations per unit volume of material) from SF to SF-CTAB@0.4 ($3.023x10^{15}$-$1.496x10^{15}$ l/m^2) suggests an increase in crystallinity[30] (**Table. 3**). The packing fraction (PF) of SF (72.113), SF-CTAB@0.2 (93.482) and SF-CTAB@0.4 (102.746) increases due to variation in their crystallite sizes (D) ranging from 18-25 nm [31]. The stacking fault ($F_{Staking}$) refers to disturbances in the normal lattice structure that arise in a layered arrangement or faults that occur in the atomic planes of a crystal. This was reported by Muniba and M. Khalid et. al. [32]. The obtained $F_{Staking}$ decreased and caused lower disturbances in the normal lattice structure, from 0.4482 to 0.4463 for SF and SF-CTAB@0.4, respectively. The specific surface area (S_{Area}) of SF ($60.902x10^3$m^2/g) is higher than CTAB@0.2 (47

$x10^3m^2/g$) and 0.4($42.536x10^3m^2/g$) corresponds to a higher crystallite size of SF-CTAB@0.2 (23.579 nm) and SF-CTAB@0.4(25.846 nm) than SF (18.185 nm).

The experimental density(ρ_{exp}) and percentage porosity(%P) for SF, SF-CTAB@0.2, and SF-CTAB@0.4 was calculated by **Eq(9)-Eq(10)** and estimated in **Table.3.**

$$\rho_{\exp} = \frac{W}{\pi r^2 t} \qquad (9)$$

Where W-wt. of pallet, t-thickness, and r-radius of the pallet

$$Porosity(P) = \frac{\rho_{X-ray} - \rho_{Exp}}{\rho_{X-ray}} X100\% \qquad (10)$$

The X-ray density ($\rho_{X\text{-}ray}$) is a measure of the number of pores in a material, which significantly impacts its electrical properties. From **Table.3**, the prepared SF-CTAB@0.4 (5.457g/cm^3) was found to be higher compared to SF-CTAB@0.2 (5.414 g/cm^3) and SF (5.417 g/cm^3) is solely a result of the lattice constant (a) of prepared material.

Table 3: Dislocation density(δ), Strain(ε), Packing factor (PF), X-ray density(ρX-ray), Experimental density(ρexp), Stacking fault (Fstacking), Specific surface area (SArea) and % porosity of prepared SF, SF-CTAB@0.2 and SF-CTAB@0.4 nano ferrite

Samples	δ ($10^{15}1/m^2$)	ε (10^{-3})	*PF*	$\rho_{X\text{-}ray}$ (g/cm^3)	ρ_{exp} (g/cm^3)	$F_{stacking}$	S_{Area}(10^3 m^2/g)	*%P*
SF	3.023	6.240	72.113	5.417	2.861	0.4482	60.902	47.181
SF-CTAB@0.2	1.798	4.813	93.482	5.414	3.190	0.4467	47.000	41.078
SF-CTAB@0.4	1.496	4.383	102.746	5.457	3.253	0.4463	42.536	40.388

It is a well-known fact that sample pores have a significant impact on experimental density. The experimental density (ρ_{exp}) for SF to SF-CTAB@0.4 was found to be lower (2.861-3.253 g/cm^3) than the X-ray density (5.414-5.457 g/cm^3) due to the presence of pores formed during material preparation. [33].

The stability of initially nucleated nano ferrite particles is determined by their porosity, as reported by S. Ikram et al. [34]. The addition of CTAB decreased the porosity of prepared nano ferrites due to an increase in crystallite size and a reduction of grain boundaries[35]. **Table. 3** shows a decrease in the porosity of SF from 47.181 to 40.388 while the crystallite size increased from 18.185 to 25.846 nm.

Other important microstructural parameters such as ionic radii at tetrahedral (r_A) and octahedral (r_B) sites, cation-anion distances(bond length) at tetrahedral (d_{AX}) and octahedral sites (d_{BX}), magnetic ion distances(hopping length) at tetrahedral (d_A) and octahedral sites (d_B) and inter-atomic distances, shared tetrahedral edge (d_{AXE}), shared octahedral edge length (d_{BXE}), and unshared octahedral edge length (d_{BXEU}) which

significantly affect the structural, magnetic and dielectric properties were evaluated through **Eq. (11)-Eq. (20)** and estimated in **Table .4** and **Table.5**

$$r_A = (u - \frac{1}{4})a\sqrt{3} - R_0 \quad (11)$$

$$r_B = (\frac{5}{8} - u)a - R_0 \quad (12)$$

$$d_{AX} = \left(u - \frac{1}{4}\right)a\sqrt{3} \quad (13)$$

$$d_{BX} = a\left(3u^2 - \frac{11}{4}u + \frac{43}{64}\right)^{1/2} \quad (14)$$

$$d_A = a\frac{\sqrt{3}}{4} \quad (15)$$

$$d_B = a\frac{\sqrt{2}}{4} \quad (16)$$

$$d_{AXE} = a\sqrt{2}(2u - \frac{1}{2}) \quad (17)$$

$$d_{BXE} = a\sqrt{2}(1 - 2u) \quad (18)$$

$$d_{BXEU} = a[4u^2 - 3u + \frac{11}{16}]^{1/2} \quad (19)$$

Where, u and R_0 are oxygen positional parameter (u = 0.384 Å) and radius of oxygen (R_o =1.32 Å) for spinel ferrite.

Table 4: Tetrahedral and Octahedral ionic radii (rA and rB), Bond length on tetrahedral and octahedral sites (dAX and dBX), Hopping length on tetrahedral and octahedral sites (dA and dB), Tetrahedral edge(dAXE), Shared Octahedral edge(dBXE) and Unshared Octahedral edge (dBXEU) of prepared SF, SF-CTAB@0.2 and SF-CTAB@0.4 nano ferrite

Sample	r_A (Å)	r_B (Å)	d_{AX} (Å)	d_{BX} (Å)	d_A (Å)	d_B (Å)	d_{AXE} (Å)	d_{BXE} (Å)	d_{BXEU} (Å)
SF	0.6204	0.6956	1.9404	2.0181	3.6215	2.9566	3.1698	2.7433	2.9607
SF-CTAB@0.2	0.6207	0.6960	1.9407	2.0185	3.6222	2.9572	3.1705	2.7438	2.9613
SF-CTAB@0.4	0.6156	0.6907	1.9356	2.0132	3.6126	2.9493	3.1621	2.7366	2.9535

Table 4 shows that the r_A value for SF-CTAB@0.2 (0.6207 Å) is slightly higher than SF (0.6204 Å) and SF-CTAB@0.4 (0.6156 Å), indicating an expansion of the tetrahedral (A) site resulting from an increase in tetrahedral ions. This expansion causes the A-site cations to move away from the tetrahedral coordination, thereby increasing the d_{AXE} and d_{AX} of SF-CTAB@0.2 compared to SF and SF-CTAB@0.4.Similarly, $d_{B,}$ and d_{BXE} was found to be higher for SF-CTAB@0.2 than SF and SF-CTAB@0.4 corresponds

to increased movement of anions away from the octahedral site, thus increasing the distance between octahedral cation-anion (d_{BX}) and the distance between the shared anions (d_{BEX}) [36]. The observed smaller d_{AX} (1.9404-1.9407 Å) than d_{BX} (2.0181-2.0185 Å) ascribed to a larger overlapping of orbitals of Fe^{3+} and O^{2-} at the tetrahedral (A)site.

The magnetic interactions through structural parameters (cation-anion magnetic interaction (p, q, r, s) and cation-cation magnetic interaction (b, c, d, e, f)) were calculated using **Eq. (20)-Eq. (28)** and estimated in **Table.5** [37].

$$b = \sqrt{2}\left(\frac{a}{4}\right) \quad (20)$$

$$c = \sqrt{11}\left(\frac{a}{8}\right) \quad (21)$$

$$d = \sqrt{3}\left(\frac{a}{4}\right) \quad (22)$$

$$e = \sqrt{3}\left(\frac{3a}{4}\right) \quad (23)$$

$$f = \sqrt{6}\left(\frac{a}{4}\right) \quad (24)$$

$$p = \left(\frac{5}{8} - u\right)a \quad (25)$$

$$q = a\sqrt{3}\left(u - \frac{1}{4}\right) \quad (26)$$

$$r = a\sqrt{11}\left(u - \frac{1}{4}\right) \quad (27)$$

$$s = a\sqrt{3}\left(\frac{u}{3} + \frac{1}{8}\right) \quad (28)$$

Table 5: Cation-anion (p, q, r, s) and cation-cation (b, c, d, e, f) of prepared SF, SF-CTAB@0.2 and SF-CTAB@0.4 nano ferrite

Sample	**p** (A°)	**q** (A°)	**r** (A°)	**s** (A°)	**b** (A°)	**c** (A°)	**d** (A°)	**e** (A°)	**f** (A°)
SF	2.0156	1.9404	3.7168	3.6650	2.9566	3.4667	3.6215	10.8645	5.1211
SF-CTAB@0.2	2.0160	1.9407	3.7176	3.6657	2.9572	3.4674	3.6222	10.8667	5.1221
SF-CTAB@0.4	2.0107	1.9356	3.7077	3.6560	2.9493	3.4582	3.6126	10.8379	5.1086

Table.5 demonstrates the cation -anion (p, q, r, s) and cation -cation (b, c, d, e, f*)* interaction for SF-CTAB@0.2 are slightly higher than SF and SF-CTAB@0.4 in accordance with higher unit cell volume (V) of SF-CTAB@0.2 (585.430 $Å^3$**)** than that of SF **(**585.074 $Å^3$**)** and SF-CTAB@0.4 (580.782 $Å^3$)[38].

The bond angles (θ_1, θ_2, θ_3, θ_4, θ_5) was used to investigate tetrahedral-tetrahedral (A-A), tetrahedral-octahedral (A-B) and Octahedral-Octahedral (B-B) magnetic interactions calculated using **Eq. (29)-Eq. (33)**

$$\theta_1 = \cos^{-1}\left(\frac{p^2+q^2-c^2}{2pq}\right) \qquad (29)$$

$$\theta_2 = \cos^{-1}\left(\frac{p^2+r^2-c^2}{2pr}\right) \qquad (30)$$

$$\theta_3 = \cos^{-1}\left(\frac{2p^2-b^2}{2p^2}\right) \qquad (31)$$

$$\theta_4 = \cos^{-1}\left(\frac{p^2+s^2-f^2}{2ps}\right) \qquad (32)$$

$$\theta_5 = \cos^{-1}\left(\frac{r^2+q^2-d^2}{2rq}\right) \qquad (33)$$

Table 6: - Bond angles θ_1, θ_2, θ_3, θ_4 and θ_5 of prepared SF, SF-CTAB@0.2 and SF-CTAB@0.4 nano ferrite

Sample	θ_1 (deg)	θ_2 (deg)	θ_3 (deg)	θ_4 (deg)	θ_5 (deg)
SF	122.3912	66.9798	94.3493	126.2239	71.9699
SF-CTAB@0.2	122.3957	66.9786	94.3498	126.2244	71.9683
SF-CTAB@0.4	122.3905	66.9793	94.3446	126.2256	71.9693

From **Table.6**, it can be observed that SF with a value of θ_5 at 71.9699° has a greater strengthening effect on the tetrahedral-tetrahedral (A-A) interaction compared to SF-CTAB@0.2 (71.9683°) and SF-CTAB@0.4 (71.9693°). It was found that the values of θ_3 and θ_4 relate to interactions between octahedral structures (B-B). The larger value of θ_3 for SF-CTAB@0.2 (94.3498°) suggests stronger bonding compared to SF (94.3493°) and SF-CTAB@0.4 (94.3446°). Additionally, as θ_4 increases from SF to SF-CTAB@0.4 (from 126.2239 to 126.2256°), it indicates a variation in the B-B interaction with CTAB. The A-B interactions related to $\theta_1$for SF-CTAB@0.2 (122.3957°) are stronger compared to SF (122.3912°) and SF-CTAB@0.4 (122.3905°). On the other hand, weak A-B interactions were observed for θ_2 in SF-CTAB@0.2 (66.9786°) and SF-CTAB@0.4 (66.9793°) compared to SF (66.9798°), as the strength depends on the bond angles and bond length between the cations and cation-anion. [39].

2. **Vibrational Spectroscopy:** The vibrational spectra of prepared SF, SF-CTAB@0.2, and SF-CTAB@0.4 nano ferrite demonstrated in **Figure.2**.The vibrations recorded by FTIR around 400-500 cm^{-1} and 500-600 cm^{-1} confirm the function group (Fe-O) of spinel ferrite with octahedral [B] and tetrahedral(A) sites respectively. The recorded higher vibrations ν_1 at 574.002 cm^{-1},580.016 cm^{-1},581.005 cm^{-1} and lower vibrations ν_2 at 486.018 cm^{-1},470.002 cm^{-1},452.988 cm^{-1} correspond to tetrahedral (A) and octahedral[B] position of prepared SF, SF-CTAB@0.2, and SF-CTAB@0.4 accordingly. The increase

in ν_1 from 574.002-581.005 cm^{-1} and decrease in ν_2 from 486.018-452.988 cm^{-1} for SF-SFCTAB@0.4 mainly due to the difference in bond length d_{AX} and d_{BX} (see **Table .4**) [40]. The strength of the bond at a tetrahedral site (A) and octahedral site [B] was determined by the force constant of the Fe-O bond using **Eq.(34)** and **Eq.(35)** and the estimated values are listed in **Table 7**.

$$K_t = 4\pi^2 c^2 \nu_1^2 m \qquad (34)$$

$$K_o = 4\pi^2 c^2 \nu_2^2 m \qquad (35)$$

Where c is the light velocity (3×10^8 m/s), ν_1 and ν_2 are the frequency of the vibrational band at tetrahedral (A) and octahedral[B] sites, and m is the reduced mass of Fe and O ions, respectively.

Table 7: Tetrahedral vibration (ν_1), Octahedral vibration (ν_2), Force constant at tetrahedral and octahedral positions (K_t and K_o), and Debye Temperature (θ_D) of prepared SF, SF-CTAB@0.2, and SF-CTAB@0.4 nano ferrite

Sample	ν_1 (cm^{-1})	ν_2 (cm^{-1})	K_t (N/m)	K_o (N/m)	ν_{av} (cm^{-1})	θ_D (*K*)
SF	574.002	486.018	241.460	173.110	530.01	757
SF-CTAB@0.2	580.016	470.002	246.546	161.889	525.00	750
SF-CTAB@0.4	581.005	452.988	247.387	150.380	516.99	739

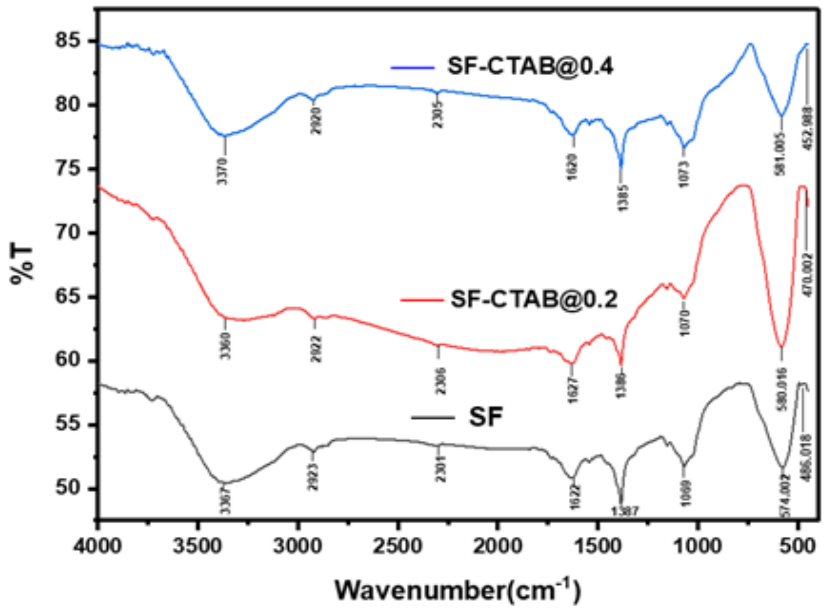

Figure 2: FTIR of prepared SF, SF-CTAB@0.2 and SF-CTAB@0.4 nano ferrite

According to **Table 7**, it is observed that the force constant at the tetrahedral site (K_t) has increased from 241.460 -247.387 N/m, while the force constant at the octahedral site (Ko) has decreased from 173.110 -150.380 N/m for SF to SF-CTAB@0.4. This

change can be attributed to the position of the spinel crystal lattice or the vibration band (ν_1 and ν_2) at their respective sites [41]. The Debye temperature (θ_D) was used to measure a lattice vibration of prepared SF, SF-CTAB@0.2, and SF-CTAB@0.4 using **Eq.(36)**

$$\theta_D = \frac{hc\nu_{av}}{k_B} \qquad (36)$$

where h is Plank constant (h = 6.626×10−34 J·s), k_B is Boltzmann constant (k_B =1.3806×10−23 J·K^{-1}), c is velocity of light (c = 3×10^8 m/s) and $\nu_{av} = \frac{\nu_1 + \nu_2}{2}$.

The obtained θ_D was found to decrease from 757 K to 739 K for SF, indicating a decrease in lattice vibration due to CTAB coating.

3. Magnetic Analysis

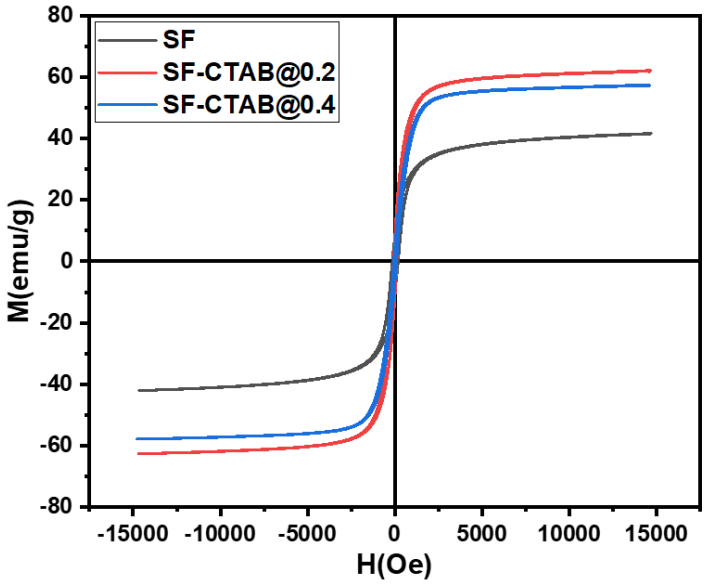

Figure 3: M-H loop of prepared SF(a), SF-CTAB@0.2(b), and SF-CTAB@0.4(c) nano ferrite

The magnetic properties of SF, SF-CTAB@0.2, and SF-CTAB@0.4 nano spinel ferrite were analyzed via an M-H loop recorded within ± 15kOe. All prepared nano ferrites exhibit a well-saturated hysteresis area indicating their soft magnetic nature(**Figure.3**). The magnetic saturation (Ms), retentivity (Mr), and coercivity (Hc) of SF, SF-CTAB@0.2, and SF-CTAB@0.4 are listed in the **Table.8**.

Table 8: Magnetic Saturation (*Ms*), Retentivity (*Mr*), Coercivity (*Hc*), Magneto-crystalline anisotropy (*K*), Bohr's magneton $\eta_B(\mu_B)$ and squareness ratio (*Mr/Ms*) of prepared SF, SF-CTAB@0.2, and SF-CTAB@0.4 nano ferrite

Sample	***Ms*** (emu/g)	***Mr*** (emu/g)	***Hc*** (Oe)	***K*** (erg/cm^3)	$\eta_B(\mu_B)$	***Mr/Ms***
SF	41.469	9.006	165.661	7010	1.7709	0.217
SF-CTAB@0.2	61.880	9.730	93.724	5918	2.6426	0.157
SF-CTAB@0.4	57.293	5.526	75.231	4398	2.4467	0.096

From **Table.8**, it was observed that, *Ms* for SF (41.469 emu/g) found to be lower than SF-CTAB@0.2 (61.880 emu/g) and SF-CTAB@0.4 (57.293 emu/g) assign to smaller crystallite size (D)of SF (18.185 nm) as that of SF-CTAB@0.2 (23.579 nm) and SF-CTAB@0.4 (25.846 nm). Additionally, the lower Ms value for SF-CTAB@0.4 compared to SF-CTAB@0.2 may be attributed to the canting of spins on the surface of SF-CTAB@0.4 [42]. The decreased coercivity(*Hc*) from 165.661 Oe to 75.231Oe for SF to SF-CTAB@0.4 corresponds to decline trend of dislocation density(δ)[43] from SF to SF-CTAB@0.4 (3.023x10^{15} 1/m^2 to 1.496 x10^{15} 1/m^2) and well known inverse relationship of Hc and the crystallite size (D)[44].The lower magnetic retentivity(*Mr*) for SF-CTAB@0.4 (5.526 emu/g) was recorded compared to SF-CTAB@0.2(9.730 emu/g) and SF(9.006) attributed to lower stain for SF-CTAB@0.4(4.383 x10^{-3}) as that of SF-CTAB@0.2(4.813 x10^{-3}) and SF(6.240 x10^{-3})[45].

The anisotropy field is a measure of the forces of crystal anisotropy that bind the magnetization to a particular direction. The magnetic moment due to the exchange of magnetic cations at tetrahedral sites rather than octahedral sites and magnetocrystalline anisotropy is calculated by **Eq. (37)-Eq. (38)**

$$\eta_B = M^* M_S / 5585 \qquad (37)$$

$$K = \frac{H_C M_S}{0.98} \qquad (38)$$

As reported earlier, the magneto-crystalline anisotropy(*K*) corresponds to the domain wall energy of the spinel nanoferrite. Higher *K* signifies higher domain wall energy and vice-versa. The recorded decreasing *K* from SF (7010 erg/cm^3) to SF-CTAB@0.4 (4398 erg/cm^3) is due to a reduction in the spin-orbit interaction of surface metal ions and CTAB [46,47]. The obtained higher Bohr Magneton $\eta_B(\mu_B)$ for SF-CTAB@0.2 (2.6426) than SF-CTAB@0.4 (2.4467) and SF(1.7709) can be interpreted based on nonlinear or canted spin ordering. According to, M.I.A. A. Maksoud et.al, the produced strain in the tiny crystal due to radii mismatch leads to a noncollinear arrangement of surface spins in the nano range, and the diamagnetic cations leads to spin canting in the sublattice resulting in a reduction in Bohr's magneton [48].

The magnetic hardness of the prepared SF, SF-CTAB@0.2, and SF-CTAB@0.4 was described by squareness ratio (*Mr/Ms*). As previously reported, the Squareness ratio ($0.5 < Mr/Ms < 1$) signifies the more anisotropic, hard, and single-domain nature of nano

ferrite [49]. Further, if 0.05 < *Mr/Ms* < 0.5 corresponds to the particle interaction by magnetostatic couplings with pseudo-single domain, and *Mr/Ms* < 0.05 signifies the randomly oriented multi-domain nature of the nano ferrite [50-52]. The obtained squareness ratio (*Mr/Ms*) (**Table.7**) clearly indicates the pseudo-single domain nature of prepared SF, SF-CTAB@0.2, and SF-CTAB@0.4 nano ferrites and finds suitability in Multilayer Chip Inductor (MLCI) application.

4. **Dielectric Spectroscopy:** The room temperature dielectric spectroscopy of prepared SF, SF-CTAB@0.2, and SF-CTAB@0.4 was evaluated by Impedance Analyzer in the frequency range of 100 Hz -1MHz.The dielectric spectroscopic parameter ie dielectric constant (ε´), dielectric loss(ε″), loss tangent(tanδ) were estimated using relation **Eq.(39)-Eq. (40)**

$$\varepsilon' = \frac{Cd}{\varepsilon_0 A} \qquad (39)$$

$$\tan\delta = \frac{\varepsilon''}{\varepsilon'} \qquad (40)$$

Where, ε´ = dielectric constant, ε″ = dielectric loss factor, tanδ= loss tangent,
ε_0 = free space permittivity = 8.854 x 10^{-12} F.m^{-1}
d = thickness of the pellet in mm
C = capacitance of the pellet in Farad

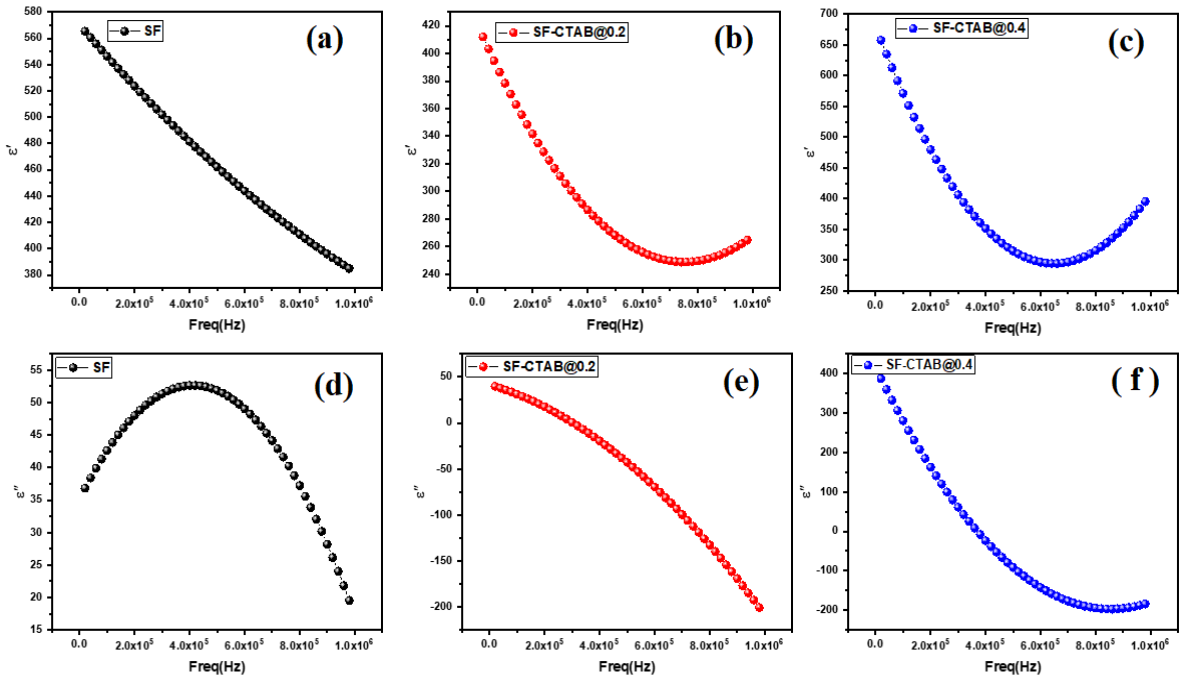

Figure 4: Dielectric constant and Dielectric loss of SF (a and d),SF-CTAB@0.2(b and e) and SF-CTAB@0.4(c and f) nano ferrite

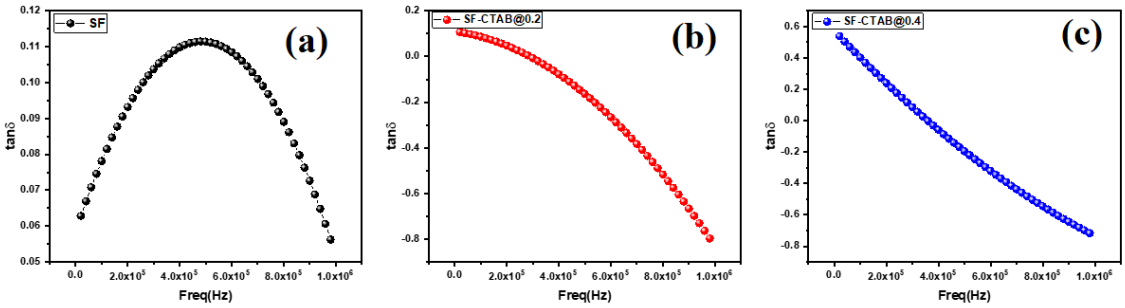

Figure 6: loss tangent of prepared SF (a),SF-CTAB@0.2(b) and SF-CTAB@0.4(c) nano ferrite

As shown in **Figure.4(a,b,c)**, the ε´ for SF found to be decreased linearly with frequency indicating the dielectric poles are able to follow the frequency . Same decline trend of ε´ was found for SF-CTAB@0.2 (**Fig.b**) and SF-CTAB@0.4 (**Fig.c**) up to $8x10^5$Hz after that ε´ slightly increases at higher frequency also known as resonance phenomena observed due to the energy coupling assign to intrinsic property associated to lattice distortion of the crystal structure of prepared nano ferrite[53]. According to H. S. Aziz et.al, when rotational frequency of electron around their axis becomes equal to the applied frequency resulting coupling of energy generates a resonance phenomenon due to the vacancy or pores leading to the space charge polarization in low-frequency regions while high-frequency resonance is due to the atomic and electronic polarization[54]. The difference in magnitude of ε´ for SF, SF-CTAB@0.2, and SF-CTAB@0.4 corresponds to the variation in Fe^{2+} concentration as a result of cation distribution at respective sites [55].

The room temperature dielectric loss(ε″) of prepared SF, SF-CTAB@0.2, and SF-CTAB@0.4 were plotted against the 100 Hz-1MHz and shown in **Figure 4(d,e,f)**. The dielectric loss generally decreases with increasing frequency and the same trend was observed for SF-CTAB@0.2, and SF-CTAB@0.4 because of a decrease in polarization as a result of grain boundary effect [56]. For the prepared SF, ε″ gradually increased from 36 to 52 and then reached 19 with higher frequency because dielectric losses in ferrites generally appear in resistivity measurements in that materials with low resistivity show high dielectric losses and vice versa[57]. The loss tangent (tanδ) shows the nearly same behaviors as that of ε″ for SF, SF-CTAB@0.2, and SF-CTAB@0.4 accordingly. The higher and lower dielectric loss tangent with the lower and higher frequency due to a strong association between the dielectric behavior of ferrites and the conduction mechanism. Further, the exponential and linear decrease of tan δ with increasing frequency is correlated with the hopping frequency of charge carriers and externally applied electric field reported by V.Vinayak et.al[58]

IV. CONCLUSIONS

A successful preparation of $Ni_{0.3}Cu_{0.3}Zn_{0.4}Fe_2O_4$ and CTAB-coated $Ni_{0.3}Cu_{0.3}Zn_{0.4}Fe_2O_4$ spinel nano ferrite was achieved through the co-precipitation method. The microstructural and magnetic properties of the material were investigated using X-ray diffraction (XRD) and a Vibrating Sample Magnetometer (VSM). The recorded X-ray diffraction pattern confirms the formation of spinel nano ferrite with space group Fd-3m. The

distribution of cations, as determined by the intensity ratio, has a noticeable impact on the size (18-25 nm), strain ($6.240x10^{-3}$-$4.383\ x10^{-3}$), magnetic interactions (AA, BB, and AB), and other microstructural parameters of all the prepared nano ferrites. This effect is particularly significant when CTAB is used as a capping agent/surfactant. The magnetic isotherm (M-H loop) recorded modifications in Ms, Mr, and Hc. The Mr/Ms value (0.217-0.096) indicates that the prepared nano ferrite is of a pseudo-single domain nature. This makes it suitable for use in multilayer ferrite cheap inductor (MLCI) applications.

V. ACKNOWLEDGMENT

The authors express gratitude to STIC Cochin for conducting the XRD analysis, SAIF Lucknow for performing the FTIR studies, and CIF (IIT Guwahati) for undertaking the Room Temperature Magnetic analysis. The college administration's support and provision of necessary facilities for the research are also acknowledged.

REFERENCES

[1] H. Qin, Y. He, P. Xu, D. Huang, Z. Wang, H. Wang, Z. Wang, Y. Zhao, Q. Tian and C. Wang, Spinel ferrites (MFe_2O_4): Synthesis, improvement and catalytic application in environment and energy field, *Adv. Colloid Interface Sci.*294(2021)102486

[2] S. P. Gubin, Y. A. Koksharov, G. B. Khomutov and G. Y. Yurkov, Magnetic nanoparticles: Preparation, structure and properties, *Russ. Chem. Rev.* 74 (2005) 489–520.

[3] A. P. Guimarães, Principles of Nanomagnetism, *Springer: Berlin/Heidelberg, Germany* (2009).

[4] G. Bertotti, "Hysterisis in Magnetism: For Physicists, Materials Scientists, and Engineers," *Academic Press-Elsevier: Waltham, MA, USA* (1998).

[5] J. Frenkel and J. Doefman , Spontaneous and induced magnetisation in ferromagnetic bodies, *Nature* 126 (1930) 274–275.

[6] C. Kittel, "Theory of the structure of ferromagnetic domains in films and small particles," *Phys. Rev.* 70 (1946) 965–971.

[7] S. Mørup, M. F. Hansen, C. Frandsen, D. Andrews, G. Scholes G. Eds. Wiederrecht, Comprehensive Nanoscience and Technology, *Elsevier: Amsterdam, The Netherlands* (2011) 437–491.

[8] C. P. Bean, J. D. Livingston, "Superparamagnetism," *J. Appl. Phys.* 30 (1959) 120S–129S.

[9] S. Bedant and W. Kleemann, Supermagnetism, *J. Phys. D* 42 (2009) 013001

[10] S.C.Tolani, A. R. Golhar and K. G. Rewatkar ,A review of morphological, structural behaviour and technological applications of ferrites, *AIP Conf. Proc* 2104, 030032 (2019)

[11] M. A. Cobos, P. Presa, I. Llorente, J. M. Alonso, A. García-Escorial, P. Marín, A. Hernando and J. A. Jimenez , Magnetic Phase Diagram of Nanostructured Zinc Ferrite as a Function of Inversion Degree δ, *J. Phys. Chem. C* 123(2019) 17472−17482

[12] C. Yang, F. Liu and T. Ren, L. Liu, H. Feng, A.Z. Wang and H. Long ,Fully integrated ferrite-based inductors for RF ICs, *Sens. Actuator A Phys.* 130-131 (2006) 365–370.

[13] S. Bae, Y.Hong, J. Lee, W. Seong, J. Kum, W. Ahn S.Park, G. S. Abo, J. Jalli, J.Park, Miniaturized Broadband Ferrite T-DMB Antenna for Mobile-Phone Applications, *IEEE Trans. Magn.* 46 (2010) 2361–2364.

[14] A. Verma, M. I. Alam, R. Chatterjee, T. C. Goel, and R. G. Mendiratta, "Development of a new soft ferrite core for power applications," *J. Magn. Magn. Mater* 300(2) (2006) 500–505.

[15] N. Channa,M. Khalid,A.D. Chandio,G. M.M. S.Akhtar,J. K. Khan,J. Ahmad,K. A. Kalhoro, Nickel-substituted manganese spinel ferrite nanoparticles for high-frequency applications, *J. Mater. Sci. Mater. Electron.*31(2020) 1661-1671

[16] P.Smitha, I. Singh, M. Najim, R. Panwar, D.Singh, V. Agarwala, G. D. Varma, Development of thin broad band radar absorbing materials using nanostructured spinel ferrites, *J. Mater. Sci. Mater. Electron* 27(2016) 7731-7737

[17] Bhamini Bhujun, Michelle T.T. Tan and Anandan S. Shanmugam, Evaluation of aluminium doped spinel ferrite electrodes for supercapacitors, *Ceram. Int.*42(2016) 6457-6466

[18] K.K. Kefeni, T. A.M. Msagati,T.T.Nkambule,B.B. Mamba, Spinel ferrite nanoparticles and nanocomposites for biomedical applications and their toxicity,Mater. Sci. Eng. C 107(2020) 110314.
[19] T. N. Pham, T. Q.Huy and A. Le , Spinel ferrite (AFe2O4)-based heterostructured designs for lithium-ion battery, environmental monitoring, and biomedical applications, *RSC Adv* 10(2020) 31622
[20] H. Q.Alijani, S. Iravani , S. Pourseyedi, M.T.Mahani, M. Barani & M. Khatami, Biosynthesis of spinel nickel ferrite nanowhiskers and their biomedical applications, *Sci. Rep.* 11(1) (2021) 17431
[21] [21] A. Benali, L. Saher, M. Bejar, E. Dhahri, M. F. P. Graca, M. A. Valente, P. Sanguino, L. A. Helguero, K. Bachari, A. M. S. Silva, B. F. O. Costa,$CoFe_2O_4$ spinel ferrite studies on permanent magnet application and cytotoxic effects on breast and prostate cancer cell lines, *Mater Sci: Mater Electron* **34**, 53 (2023)
[22] S. B. Somvanshi, P. B. Kharat, T. S. Saraf, S. Somwanshi, S.B. Shejul and K. M. Jadhav, Multifunctional nano-magnetic particles assisted viral RNA-extraction protocol for potential detection of COVID-19, *Mater. Res. Innovations* 25(3) (2021) 169-174
[23] Ashkan Bigham, Firoozeh Foroughi, Mehdi Motamedi, M. Rafienia, *Ceram. Int 44(10) (2018)* 11798-11806
[24] A. Lassoued,M.Ben hassine,F. Karolak, B. Dkhil ,S. Ammar ,A.Gadri, Synthesis and magnetic characterization of Spinel ferrites MFe2O4 (M=Ni, Co, Zn and Cu) via chemical co-precipitation method, *J. Mater. Sci.: Mater. Electron.*28(24) (2017) 18857-18864
[25] M. Haneef , I. H. Gul1 ,M. Hussain and I. Hassan, Investigation of Magnetic and Dielectric Properties of Cobalt Cubic Spinel Ferrite Nanoparticles Synthesized by CTAB-Assisted Co-precipitation Method, *J. Supercond. Nov. Magn.* 34 (2021) 1467-1476
[26] P.P. Hankare , R.P. Patil a , U.B. Sankpal ,S.D. Jadhav , P.D. Lokhande , K.M. Jadhav , R. Sasikala , Investigation of structural and magnetic properties of nanocrystalline manganese substituted lithium ferrites, *J. Solid State Chem.* 182 (2009) 3217–3221
[27] B.P. Ladgaonkar and A.S. Vaingankar, X-ray diffraction investigation of cation distribution in CdxCUl_xFe204 ferrite system,J.*Mater. Chem. Phys.* 56 (1998) 280-283
[28] B. B. V. S. Vara Prasad, K. V. Ramesh and Adiraj Srinivas, Structural and Magnetic Studies of Nano-crystalline Ferrites MFe2O4 (M = Zn, Ni, Cu, and Co) Synthesized Via Citrate Gel Autocombustion Method, *J Supercond Nov Magn.*30(12)(2017) 3523-3535
[29] M. Haneef, I. H. Gul, M. Hussain and I. Hassan, Investigation of Magnetic and Dielectric Properties of Cobalt Cubic Spinel Ferrite Nanoparticles Synthesized by CTAB-Assisted Co-precipitation Method, J Supercond Nov Magn, **34**(2021) 1467–1476 .
[30] R. Verma, A. Chauhan, K. M. Batoo, R. Kumar, M. Hadhi, and Emad H. Raslan, Effect of calcination temperature on structural and morphological properties of bismuth ferrite nanoparticles, Ceram. Int. 47(3) (2021) 3680-3691.
[31] S. Ikram, J. Jacob, K. Mehboob, K. Mahmood, M. S. Nawaz, and N. Amin. Relationship of Various Structural Parameters with Magnetic Behavior of Stoichiometric Tb^{3+} and Dy^{3+} Co-substituted $NiFe_2O_4$ Nanostructures. *J Supercond Nov Magn* 34 (2021) 1753–1758 .
[32] Muniba, M. Khalid, A. D. Chandio, M. S. Akhtar, J. K. Khan, G. Mustafa, N. U. Channa, Z. A. Gilani, and HM Noor ul Huda Khan Asghar, Aluminum substitution in Ni-Co based spinel ferrite nanoparticles by sol–gel auto-combustion method, *J. Electron. Mater* 50 (2021) 3302-3311.
[33] D.V. Kurmude ,R.S. Barkule ,A.V. Raut , D.R. Shengule and K.M. Jadhav, X-Ray Diffraction and Cation Distribution Studies in Zinc-Substituted Nickel Ferrite Nanoparticles, *J Supercond Nov Magn, **27(2014)** 547–553* .
[34] S. Ikram, F. Ashraf, M. Alzaid, K. Mahmood,N. Amin and S. Ali Haider, Role of Nature of Rare Earth Ion Dopants on Structural, Spectral, and Magnetic Properties in Spinel Ferrites, J. Supercond. Nov. Magn.34(2020) 1745-1751.
[35] M.A. Hakim, S. K. Nath, S.S. Sikder and K. H. Maria, Cation distribution and electromagnetic properties of spinel type Ni–Cd ferrites, J. Phys. Chem. Solids .74 (2013) 1316–1321
[36] M. Satalkara , S N Kane, On structural studies and cation distribution of La added Zn-Ni-Mg-Cu spinel nano ferrite, J. Phys. Conf. Ser.755(2016) 012047
[37] P. Thakur, R. Sharma, M. Kumar, S C Katyal, N S Negi, N. Thakur, V. Sharma and P. Sharma, Superparamagnetic La doped Mn–Zn nano ferrites: dependence on dopant content and crystallite size, Mater. Res. Express 3(7) (2016) 075001.
[38] [38] K.A. Mohammed , A.D. Al-Rawas , A.M. Gismelseed , A. Sellai, H.M. Widatallah , A. Yousif , M.E. Elzain and M. Shongwe , Infrared and structural studies of Mg1–xZnxFe2O4 ferrites, Phys. B: Condens. Matter 407(2012) 795-804

[39] V.K. Lakhani, T.K. Pathak, N.H. Vasoya and K.B. Modi, Structural parameters and X-ray Debye temperature determination study on copper-ferrite-aluminates, Solid State Sci.13(2011) 539-547
[40] S. Dasa , M. Bououdinab , C. Manoharana, The influence of cationic surfactant CTAB on optical, dielectric and magnetic properties of cobalt ferrite nanoparticles, Ceram. Int. 46(8) (2020)11705-11716
[41] S. N. Kane , S. Raghuvanshi , M. Satalkar , V. R. Reddy , U. P. Deshpande , T. R. Tatarchuk and F. Mazaleyrat, Synthesis, Characterization And Antistructure Modeling Of Ni Nano Ferrite, AIP Conf Proc .1953(1) (2018) 030089
[42] A.Anwar, S. Zulfiqar, M.A. Yousuf, S. A. Ragab , M.A.Khan, I. Shakir and M. F.Warsi, Impact of rare earth Dy+3 cations on the various parameters of nanocrystalline nickel spinel ferrite, j mater res technol. 9(3) (2020) 5313–5325
[43] Jiyu Hu, Yongqing Ma, Xucai Kan, Chaocheng Liu, Xian Zhang, Rui Rao, Min Wang and Ganhong Zheng,Investigations of Co substitution on the structural and magnetic properties of Ni-Zn spinel ferrite, J. Magn. Magn. Mater. 513 (2020) 167200.
[44] M.F.Sarac, Magnetic, Structural, and Optical Properties of Gadolinium-Substituted $Co_{0.5}Ni_{0.5}Fe_2O_4$ Spinel Ferrite Nanostructures. J Supercond Nov Magn 33 (2020)397–406
[45] M. M. L. Sonia, S. Anand, V. M. Vinosel, M. A. Janifer, S. Pauline, A. Manikandan, Effect of lattice strain on structure, morphology and magneto-dielectric properties of spinel NiGdxFe2-xO4 ferrite nano-crystallites synthesized by sol-gel route, J. Magn. Magn. Mater. 466(2018) 238-251.
[46] R D Raland and J P Borah ,Efficacy of heat generation in CTAB coated Mn doped ZnFe2O4 nanoparticles for magnetic hyperthermia , J. Phys. D: Appl. Phys. 50 (2017) 035001
[47] L. Kumar and M. Kar, Influence of Al^{3+} concentration on the crystal structure and magnetic anisotropy of nanocrystalline spinel cobalt ferrite, J. Magn. Magn. Mater. 323 (2011) 2042–2048
[48] M.I.A.A.Maksoud, A.El-Ghandour , A.H. Ashour , M.M. Atta , S. Abdelhaleem , A.H. El-Hanbaly , R. A.Fahim, S. M. Kassem , M.S. Shalaby, A.S. Awed , La^{3+} doped LiCo0.25Zn0.25Fe2O4 spinel ferrite nanocrystals: Insights on structural, optical and magnetic properties, J. Rare Earths. 39 (2021) 75-82
[49] V.Badwaik, D. Badwaik, V. Nanoti, and K. Rewatkar, Study of some structural and magnetic properties of Sr 2 Me 2 Fe 11 (SnCo) 0.5 O 22 nanoferrites, Int J Know Eng 3 (2012) 58-60.
[50] V. V. Warhate and D. S. Badwaik, Structural, magnetic and thermo-magnetic properties of NiMn Y-Type strontium nano-hexaferrites, J. Alloys Compd. 818 (2020) 152830.
[51] S.M. Suryawanshi, D.S. Badwaik, B.S. Shinde , K.D. Gaikwad, M. Shkir, K.V. Chandekar, S. Gundale, A comprehensive study on structural, magnetic and dielectric properties of $Ni_{0.3}Cu_{0.3}Zn_{0.4}Fe_{1.8}Cr_{0.2}O_4$ nanoparticles synthesized by sol-gel auto combustion route, J. Mol. Struct.1272(2023) 134173
[52] S.R.Daf, D.S.Badwaik, S.M.Suryawanshi,V.S.Harode, and B.R.Balbudhe,Physical, spectroscopic and antibacterial investigation of Mg0. 3Zn0. 5Mn0. 2Fe2O4 via temperature dependent hydrothermal approach. J. Magn. Magn. Mater. 567(2023)170346.
[53] H.S.Aziz, S.Rasheed, R.A.Khan, A.Rahim, J.Nisar, S.M. Shah, F.Iqbal and A.R. Khan , Evaluation of electrical, dielectric and magnetic characteristics of Al–La doped nickel spinel ferrites, RSC Adv., (6) 2016 6589-6597
[54] H.S.Aziza , R.A.Khana,F.Shaha , B.Ismaila , J. Nisarb , S. M. Shah , A. Rahim, A.R. Khan, Improved electrical, dielectric and magnetic properties of Al-Sm co-doped NiFe2O4 spinel ferrites nanoparticles, J. mater. sci. eng. B,243(2019) 47-53
[55] N. Sivakumar, A. Narayanasamya, J.-M. Greneche, R. Murugaraj , Y.S. Lee, Electrical and magnetic behaviour of nanostructured MgFe2O4 spinel ferrite, J. Alloys Compd. 504 (2010) 395–402
[56] H. M. T. Farid, I. Ahmad , I.Ali , S.M. Ramay, A. Mahmood, G. Murtaza, Dielectric and impedance study of praseodymium substituted Mg-based spinel ferrites, J. Magn. Magn. Mater. 434 (2017) 143–150
[57] M.Gul and K. Akhtar, Synthesis and characterization of Al_ doped manganese ferrite uniform particles for high-frequency applications, J. Alloys Compd. 765(2018)1139-1147
[58] V. Vinayak, P. P. Khirade, S. D. Birajdar, R. C. Alange and K. M. Jadhav, Electrical and Dielectrical Properties of Low-Temperature-Synthesized Nanocrystalline Mg2+-Substituted Cobalt Spinel Ferrite, J Supercond Nov Magn 28 (2015) 3351–3356

